

See discussions, stats, and author profiles for this publication at: <https://www.researchgate.net/publication/43344699>

# Intracellular Uptake and Trafficking of Difluoroboron Dibenzoylmethane-Polylactide Nanoparticles in HeLa Cells

ARTICLE in ACS NANO · MAY 2010

Impact Factor: 12.88 · DOI: 10.1021/nn901385y · Source: PubMed

CITATIONS

30

READS

39

## 7 AUTHORS, INCLUDING:



[Janette Contreras](#)

University of Southern California

5 PUBLICATIONS 105 CITATIONS

SEE PROFILE



[Guoqing Zhang](#)

University of Science and Technology of China

48 PUBLICATIONS 1,385 CITATIONS

SEE PROFILE



[Cassandra L Fraser](#)

University of Virginia

110 PUBLICATIONS 3,179 CITATIONS

SEE PROFILE



[Sarah Hamm-Alvarez](#)

University of Southern California

111 PUBLICATIONS 2,464 CITATIONS

SEE PROFILE

Published in final edited form as:

ACS Nano. 2010 May 25; 4(5): 2735–2747. doi:10.1021/nn901385y.

## Intracellular Uptake and Trafficking of Difluoroboron Dibenzoylethane-Poly(lactic acid) Nanoparticles in HeLa Cells

Janette Contreras<sup>1,\*</sup>, Jiansong Xie<sup>1,\*</sup>, Yin Jie Chen<sup>2</sup>, Hua Pei<sup>1</sup>, Guoqing Zhang<sup>2</sup>, Cassandra L. Fraser<sup>2</sup>, and Sarah F. Hamm-Alvarez<sup>1,#</sup>

<sup>1</sup>Department of Pharmacology and Pharmaceutical Sciences, University of Southern California, Los Angeles, CA 90033

<sup>2</sup>Department of Chemistry, University of Virginia, Charlottesville, VA 22904

### Abstract

In this study, nanoparticles based on difluoroboron dibenzoylethane-poly(lactic acid) (BF<sub>2</sub>dbmPLA) are prepared. Polylactic acid or polylactide is a commonly used degradable polymer, while the boron dye possesses a large extinction coefficient, high emission quantum yield, 2-photon absorption, and sensitivity to the surrounding environment. BF<sub>2</sub>dbmPLA exhibits molecular weight-dependent emission properties, and can be formulated as stable nanoparticles, suggesting that its unique optical properties may be useful in multiple contexts for probing intracellular environments. Here we show that BF<sub>2</sub>dbmPLA nanoparticles are internalized into cultured HeLa cells by endocytosis, and that within the cellular milieu they retain their fluorescence properties. BF<sub>2</sub>dbmPLA nanoparticles are photostable, resisting laser-induced photobleaching under conditions that destroy the fluorescence of a common photostable probe, LysoTracker™ blue. Their endocytosis is also lipid raft-dependent, as evidenced by their significant co-localization with cholera toxin B subunit in membrane compartments after uptake, and their sensitivity of uptake to methyl- $\beta$ -cyclodextrin. Additionally, BF<sub>2</sub>dbmPLA nanoparticle endocytosis utilizes microtubules and actin filaments. Internalized BF<sub>2</sub>dbmPLA nanoparticles do not accumulate in acidic late endosomes and lysosomes, but within a perinuclear non-lysosomal compartment. These findings demonstrate the feasibility of using novel BF<sub>2</sub>dbmPLA nanoparticles exhibiting diverse emission properties for *in situ*, live cell imaging, and suggest that their endogenous uptake occurs through a lipid-raft dependent endocytosis mechanism.

### Keywords

polylactide; fluorescence; imaging agent; endocytosis; lipid rafts; CLIC-GEEC

Light emitting materials made by controlled synthetic methods and nanofabrication are useful for biological imaging and sensing. Versatile systems with easily controllable emission wavelengths are particularly desirable. Luminescent polymer-dye conjugates can be processed as nanoparticles and used to track intracellular structures and pathways.<sup>1</sup> Both fluorescence and phosphorescence emitters are widely used for these purposes. Phosphorescence is also useful for oxygen sensing, given sensitivity to oxygen quenching

#Address correspondence to: Sarah Hamm-Alvarez, Ph. D., USC School of Pharmacy, 1985 Zonal Ave, Los Angeles CA 90033, shalvar@usc.edu, 323-442-1445 O, 323-442-1390 F.

\*The first two authors contributed equally to the study

#### Supporting Information

Supporting Information Available: Supplemental figure shows time course uptake data for BNP12. This material is available free of charge via the Internet at <http://pubs.acs.org>.

through triplet energy transfer.<sup>2-4</sup> For example, dual emissive, boron biomaterial-based oxygen nanosensors are effective ratiometric tumor hypoxia imaging agents, with good spatial and temporal resolution.<sup>5</sup>

Here we prepared nanoparticles based on difluoroboron dibenzoylmethane-poly(lactic acid) or BF<sub>2</sub>dbmPLA<sup>6</sup> and explored their potential as imaging agents for cellular uptake and trafficking studies. The constituent polymer, poly(lactic acid) or polylactide (PLA)<sup>1</sup>, is commonly used as a sustainable packaging material and also is a key ingredient of diverse biomedical devices such as bioresorbable sutures and implants, drug delivery systems, and tissue engineering matrices.<sup>7</sup> The boron dye, on the other hand, exhibits a large extinction coefficient, high emission quantum yield, 2-photon absorption, and sensitivity to the surrounding environment, similar to non-polymeric  $\beta$ -diketonate<sup>8-9</sup> and BODIPY<sup>10</sup> and derivatives. Furthermore, in films and bulk materials, BF<sub>2</sub>dbmPLA exhibits molecular weight (MW) dependent luminescence as a single component macromolecular system.<sup>11</sup>

To further assess the potential of this family of dye-polymer conjugates for biology, we investigated whether nanoparticles formed from BF<sub>2</sub>dbmPLA dye-polymer conjugates<sup>12</sup> of different molecular weights retain color tunable fluorescence in aqueous environments and within the cellular milieu. Previously, nanoparticles made from BF<sub>2</sub>dbmPLA ( $M_n = 10,400$  kDa) were investigated *in vitro* and preliminary findings suggest that they accumulated in a perinuclear cellular compartment in CHO cells when they were added to the cell culture medium.<sup>12</sup> However, the optical properties of boron nanoparticles (BNPs) made from polymers of different molecular weights have not been investigated in detail, either in aqueous suspension or in cells. This study characterizes the optical properties and stability of these BNPs, tests their internalization modalities in a HeLa fibroblast-like model cell line, and begins to determine their endogenous internalization mechanisms in this system. We show here that BNPs internalized into cultured cells retain their novel optical fluorescence emission properties and are photostable *in situ*. These BNPs exhibit equivalent internalization behavior regardless of the constituent polymer molecular weight within the ranges explored in this study. Finally, BNP internalization is rapid and occurs via a lipid raft-dependent internalization pathway.

## Results and Discussion

### Nanoparticle Fabrication and Characterization

Dibenzoylmethane (dbm) modified with a primary alcohol functionality was combined with BF<sub>3</sub> to synthesize BF<sub>2</sub>dbmOH for use as an initiator in controlled, solvent-free, tin-catalyzed lactide polymerization, thus forming difluoroboron dibenzoylmethane-poly(lactic acid) (BF<sub>2</sub>dbmPLA).<sup>6</sup> By changing reaction conditions (e.g. monomer loading, polymerization times), boron polymers with different molecular weights were prepared.

Previously, experiments have shown that BF<sub>2</sub>dbmPLA fluorescence emission spectra vary depending on the molecular weight of the polymer chain.<sup>11</sup> The MW dependence of BF<sub>2</sub>dbmPLA fluorescence has been confirmed in powder and film states. To further explore the potential of utilizing the optical properties of BF<sub>2</sub>dbmPLA in biological imaging, sensing and delivery systems, and to test whether these unique color tunable optical properties persist at the nanoscale and in aqueous environments, samples of various MWs were fabricated into nanoparticles via nanoprecipitation.<sup>13-14</sup> Characterization data are

<sup>1</sup>BF<sub>2</sub>dbmPLA, difluoroboron dibenzoylmethane-poly(lactic acid); PLA, poly(lactic acid); MW, molecular weight; BNP, boron nanoparticle; DMEM, Dulbecco's modified essential medium; MBCD, methyl- $\beta$ -cyclodextrin; Lat B, latrunculin B; PBS, phosphate-buffered saline; RTP, room temperature phosphorescence; DF, delayed phosphorescence; CLIC-GEEC; clathrin-independent carrier GPI-AP-enriched early endosomal compartment dependent endocytosis; CT-B, cholera toxin B subunit

provided in Table 1. Samples are named as BNPX, where X = the molecular weight of the polymer used to fabricate the particles, 3, 6, 12, 17, and 20 kDa respectively.

In the nanoparticle state, the molecular weight dependence of BF<sub>2</sub>dbmPLA fluorescence is clearly evident upon visual inspection (Figure 1) and in emission spectra (Figure 2). Emission maxima,  $\lambda_{em}$ , range from 498–437 nm for nanoparticles composed of 3–20 kDa BF<sub>2</sub>dbmPLA. This trend is likely caused by a dye concentration effect, induced by local polarity differences arising from fluorophore-fluorophore (F-F) interactions of different strengths. In nanoparticles made from lower MW BF<sub>2</sub>dbmPLA (e.g. BNP3), the fluorophores are in closer proximity and optical dipolar interactions are stronger. The excited state is stabilized, the energy gap between ground state and excited state is reduced, and emission is red-shifted. For nanoparticles made with high MW BF<sub>2</sub>dbmPLA, in contrast, the stabilizing interaction is less, the energy gap between ground state and excited states is greater, and emission is blue-shifted. Under these conditions (i.e. lower dye/polymer loading), emission maxima parallel those observed in dilute solution.

BNPs, regardless of molecular weight, also exhibit room temperature phosphorescence (RTP). Delayed emission spectra were recorded with a ~500 ms delay after the black light excitation source was turned off. Gating allows for detection of long-lived (ms) RTP and delayed fluorescence (DF) after short-lived (ns) fluorescence has ceased (Figure 3). Delayed fluorescence results from thermal repopulation of the singlet state from the triplet excited state and appears as a high energy shoulder (~440 nm) on the main RTP peak (~510–520 nm). The DF emission follows the same trend as fluorescence ( $S_1 \rightarrow S_0$ ) and accounts for differences in the ~400–475 nm region of the emission spectra (Figure 2 and 3). It should be noted that BF<sub>2</sub>dbmPLA phosphorescence is quenched in normoxic environments, and for the cellular uptake studies, we concentrate on the fluorescence properties of these nanoparticles, utilizing confocal and multiphoton fluorescence microscopy, flow cytometry and fluorimetry.

The BNPs were also monitored over time to test for stability. After 11 weeks, the samples still exhibited MW dependent fluorescence and RTP. Both the fluorescence and delayed emission spectra for the BNPs were essentially the same after 11 weeks as at the time of fabrication. After more than a year, fluorescence and phosphorescence are still present. These results suggest that these BNPs have good shelf life with respect to optical properties and may be exploited for longer term sensing applications.

### Biological Studies: Internalization

It was previously shown that fluorescent BF<sub>2</sub>dbmPLA nanoparticles could be detected intracellularly after a 1 hr incubation in Chinese hamster ovary (CHO) cells.<sup>12</sup> To expand upon this initial observation, the intracellular distribution and emission spectra of BNPs were investigated in HeLa cells. Uptake experiments, where the cells were incubated with BNPs for 1 hr and then analyzed by multiphoton fluorescence microscopy, showed that BNPs could be detected in the perinuclear region of the cells (Figure 4). A similar distribution pattern was observed across the range of MW used to make the nanoparticles. It should be noted that BNPs fabricated with different polymer MWs are comparable in size, in the range of 77–96 nm in diameter. Since size is a critical factor affecting the uptake of these nanoparticles, it is understandable that a similar uptake and distribution pattern was observed for the BNPs of different MW. As shown in Figure 4, the emission spectra for the internalized BNPs were very close to the fluorescence emission wavelengths reported in Table 1 for the corresponding molecular weights, and remained distinct from one other. It should be noted that the particle excitation was provided by the 790 nm line of the multiphoton laser, showing the capability of these particles to exhibit multiphoton excitation and emission. This is particularly useful for in vivo applications that require the use of

multiphoton excitation because of its greater ability to penetrate thicker sections or intact tissue. As an extension of these experiments, the uptake of two different nanoparticle samples, BNP3 and BNP12, was compared to a reference, UV-excitabile fluorophore, LysoTracker™ Blue. This blue fluorescent dye, which labels highly acidic compartments within live cells and is enriched in lysosomal membranes, has an emission maxima of 422 nm. As shown in Figure 5, the intracellular distribution of BNP3 and BNP12 was quite similar to that of Lyso Tracker Blue, with all three showing significant perinuclear enrichment after 1 hr uptake.

### Biological Studies: Photostability

The BNPs retain fluorescent and phosphorescent properties even after a year on the shelf under ambient light. To further explore their photostability, BNP3 and BNP12 (<1 month since fabrication) were exposed to direct UV light for up to 24 hrs and the fluorescence intensity was measured both before and after exposure. The highly photostable LysoTracker™ Blue was used as a reference fluorophore. After direct UV light exposure for 24 hrs, approximately 50 percent of the fluorescence intensity of BNP3, and over 50 percent of BNP12, remained, while only 20-30 percent of the fluorescence intensity of LysoTracker™ Blue was detected (Figure 6A). The intracellular photostability of these nanoparticles was also examined. HeLa cells were incubated with either the highly photostable LysoTracker™ Blue or BNP (BNP3 or BNP12) for 1 hr and were imaged over time during sequential bleaching. At the zero time point, the BNP fluorescence intensity exceeded that of LysoTracker™ Blue. After approximately 9.5 min of sequential bleaching, the LysoTracker™ Blue signal was almost completely photobleached, while the BNP12 signal was still readily detected (Figure 6B). Similar results were seen for BNP3 (data not shown). Because of the strong laser power required to conduct this experiment, we began to observe cell rounding and detachment consistent with cellular damage and death at time points preceding loss of BNP fluorescence. Since we could no longer focus on nanoparticles, which moved out of the focal plane as the cells detached, we were unable to continue this experiment. However, these studies do show that BNPs were highly photostable, more so than a highly photostable live cell commercial probe, and continuously up to conditions associated with cell damage/death due to high intensity illumination.

### Biological Studies: Internalization Mechanisms

To begin to understand BNP internalization mechanisms, as well as their intracellular trafficking patterns, we investigated their intracellular localization. LysoTracker™ Red is a fluorescent acidotropic probe for tracking acidic organelles in live cells. HeLa cells were incubated with both BNP12 and LysoTracker™ Red simultaneously and then imaged. Little to no co-localization of BNP12 and LysoTracker™ Red was detected (Figure 7), suggesting that after 1 hr, the nanoparticles were not significantly localized to acidic compartments such as lysosomes, but rather to another perinuclear compartment. However the distribution pattern in apparent membrane compartments confirmed an endocytic uptake mechanism. Because BNP fluorescence was poorly retained after the sample fixation and permeabilization necessary for use of immunofluorescence detection of specific compartment markers (data not shown), we were unable to determine the identity of this non-lysosomal perinuclear membrane compartment where BNPs accumulated. Imaging nanoparticles in fixed samples has historically been very challenging, since nanoparticle fluorescence is often poorly retained after sample fixation and permeabilization.<sup>15-16</sup> Additionally, lack of potent mounting media for preserving initial and long-term fluorescence of the nanoparticles might contribute to the difficulties.

Endocytosis, the process by which internal membranes are produced by and detached from the plasma membrane lipid bilayer, can occur by multiple mechanisms. This process is

critical for the ability of the cell, through regulation of its lipid and protein plasma membrane composition, to communicate with the extracellular environment.<sup>17</sup> It is equally important for modulating uptake and cellular sorting of extracellular soluble and plasma membrane-bound constituents, including nutrients, hormones, and extracellular particulates such as nanoparticle diagnostic probes or delivery devices, into the intracellular membrane system. Understanding the mechanisms of nanoparticle endocytosis is critical for development of these novel probes as therapeutic and diagnostic tools, and for understanding how to optimize the use of a particular nanoparticle for a given situation.

For many years, the study of endocytosis has focused primarily on the pathway of clathrin-mediated endocytosis, an internalization mediated by association of adaptor proteins with membrane, recruitment of a clathrin coat, and detachment of the clathrin-coated vesicle assisted by dynamin, a GTPase acting at the cytoplasmic face.<sup>18–21</sup> More recently, a plethora of additional mechanisms have emerged that use clathrin-independent pathways, which appear in fibroblast cells to be equally prevalent with clathrin-dependent pathways, and which include caveolar endocytosis, the clathrin-independent carrier GPI-AP-enriched early endosomal compartment (CLIC/GEEC) endocytosis, arf6-dependent endocytosis, flotillin-dependent endocytosis and macropinocytosis. Many of these clathrin-independent pathways rely on the cholesterol-dependent clustering of lipid-anchored proteins into diverse microdomains.<sup>22</sup> The first of these lipid raft-dependent pathways to be studied was the caveolar endocytosis pathway, which was thought to be mediated by flask-like invaginations coated with caveolin-1 detected on the internal plasma membrane of diverse cell types, including endothelial cells, and to involve detachment of caveolae from plasma membrane by the protein, dynamin. It has now become clear that caveolae do participate in internalization of only a few markers, while they appear to be able to participate in formation of membrane extensions as well as regulation of other cellular processes.<sup>18, 22–23</sup> Other mechanisms appear to account for the variety of other lipid-raft dependent internalization mechanisms that are largely dynamin-independent and that have been detected in different systems.

For BNP uptake, several inhibitors were utilized to begin to discern the endocytic internalization mechanism. Because initial observations of rates of uptake as well as intracellular distribution suggested comparable behavior for all BNPs, we focused on BNP3 and BNP12 for detailed analysis of uptake mechanisms. The first inhibitor tested, MBCD, depletes cholesterol from the cell membranes, effectively inhibiting diverse cholesterol-dependent endocytic routes including caveolar endocytosis,<sup>24–25</sup> CLIC-GEEC endocytosis,<sup>18</sup> and, in some cases, even clathrin-mediated endocytosis.<sup>18, 26</sup> HeLa cells pre-treated with MBCD showed significantly reduced uptake of both BNP3 and BNP12 (Figure 8A) suggestive of uptake involving lipid rafts.

To determine additional features of BNP uptake through lipid raft-dependent endocytosis, we utilized fluorescently-labeled cholera toxin B (CT-B), which is known to be internalized via caveolar endocytosis and CLIC-GEEC.<sup>18</sup> Untreated and MBCD pre-treated cells were incubated with BNP12 and Alexa Fluor 594-conjugated cholera toxin subunit B (AF594 CT-B). In control cells, BNP12 and AF594 CT-B were detected intracellularly with a significant amount of co-localization. In contrast, cells pre-treated with MBCD showed reduced uptake of both BNP12 and AF594 CT-B (Figure 8B).

To try to distinguish between caveolar-dependent internalization of BNP versus their internalization via other lipid raft-dependent mechanisms, we utilized dynasore, an inhibitor of dynamin which is thought to participate in both clathrin-mediated and caveolar endocytic mechanisms.<sup>18</sup> While dynasore did not consistently impair BNP nor CT-B uptake in HeLa cells (at doses comparable to those previously used in other HeLa cells<sup>27–30</sup>), its effects on



a control ligand, Texas Red-EGF, which is known to use dynamin-dependent clathrin-mediated endocytosis<sup>31</sup> also showed little to no effects (data not shown). This finding suggested that dynasore was not acting as a reliable dynamin inhibitor under these conditions in the HeLa cells.

These data suggest that BNP uptake is dependent upon lipid rafts. Cholesterol depletion would be expected to affect multiple lipid raft-dependent endocytic pathways including caveolar endocytosis, CLIC/GEEC endocytosis and flotillin endocytosis. It has been established that CT-B traffics both through caveolar and CLIC/GEEC pathways; since it is significantly co-localized with BNP this suggest that these nanoparticles utilize similar internalization pathways. Furthermore, CT-B has been shown to traffic directly from a peripheral tubular intermediate to the Golgi apparatus.<sup>18, 24</sup> Our finding that BNPs co-localize with CT-B in a perinuclear compartment that is not labeled with the acidic organelle probe, Lysotracker, suggests that these particles, like many pathogens, may be able to exploit endogenous internalization pathways.

### Biological Studies: Role of the Cytoskeleton

Actin filaments have been implicated in various capacities in diverse endocytic pathways including caveolar and CLIC/GEEC-mediated endocytosis.<sup>18, 32</sup> Microtubules are less commonly associated with initial endocytic uptake processes but have been reported to play an important role in the sorting of endocytosed materials within endosomal compartments, in concert with motor proteins.<sup>33-34</sup> We examined the effects of nocodazole and latrunculin B (Lat B) on BNP uptake. Both agents disrupt the cell cytoskeleton and, by extension, events requiring participation by these filament systems: nocodazole is an established inhibitor of the microtubule network, promoting microtubule disassembly,<sup>33</sup> while Lat B is an inhibitor of actin filament assembly.<sup>35</sup> Both agents have previously been used successfully in HeLa cells.<sup>36-38</sup> HeLa cells pre-treated with either nocodazole or Lat B showed significantly reduced uptake of BNP<sup>12</sup> with effects readily detectable by 20 min (Figure 9A & B)). Comparable results were seen at 60 min, although the effect was less pronounced for nocodazole (data not shown). Analysis of microtubule and microfilament organization in HeLa cells treated with nocodazole or Lat B confirmed the expected disassembly of microtubules and microfilaments, respectively (Figure 9C).

While quantitative evaluation of particle uptake revealed an approximate 40% inhibition of internalization, evaluation of individual cells treated with nocodazole or Lat B suggested an even more potent inhibition. Actin filament disassembly might impact diverse endocytic pathways including caveolar or CLIC/GEEC-mediated endocytosis, consistent with the possibility of internalization via this pathway. Microtubules are more commonly associated with endosomal and post-endosomal sorting processes as well as maintenance of unique compartment morphologies;<sup>39-40</sup> their disassembly by nocodazole might affect the dynamics of intracellular sorting, thus increasing the efficiency of recycling through impairment of post-endocytic processing.

The abundance of nanoparticle formulations, sizes, shapes, and compositions has provided a series of hurdles to the comprehensive understanding of their uptake properties.<sup>41</sup> Consensus exists in the literature about the features of nanoparticles that are important for their uptake: size and surface charge.<sup>42-46</sup> While the specific effects of size and surface charge are debatable, it has been shown that nanoparticles with positive surface charge are generally more readily endocytosed because of their affinity for the negatively charged plasma membrane.<sup>46-47</sup> The use of common cationic liposomal formulations, essentially primitive nanoparticles, for efficient cell transfection lends credence to this observation.<sup>47-48</sup> However, it has been reported that endocytosis of cationic liposomes is significantly reduced in cells enriched in lipid raft markers such as GM-1,<sup>49</sup> suggesting that lipid raft

domains may have an underlying preference for negatively-charged nanoparticles. Since the BNPs studied here are likely negatively charged (based on the inclusion of PLA which is known to form a negatively charged nanoparticle<sup>44</sup>) and appear to be internalized using lipid raft-dependent processes, this suggests the need for further study of the factors governing charge interaction at lipid rafts. A schematic representation of their internalization pathway is depicted in Figure 10.

Nanoparticle endocytosis can occur in a variety of ways. In fact, a single type of nanoparticle can employ multiple endocytic routes depending on its size. For example, carboxyl-modified fluorescent polystyrene nanoparticles that are 24 nm in diameter were able to enter HeLa cells via a nonclassical (clathrin-, caveolin- and cholesterol-independent) pathway while equivalently composed 43 nm nanoparticles entered cells predominantly via clathrin-mediated endocytosis.<sup>50</sup> PLA and polylactide-polyglycolide (PLGA) nanoparticles have been shown to enter vascular smooth muscle cells through a combination of fluid phase pinocytosis and clathrin-mediated endocytosis.<sup>44, 51-52</sup> Cationic poly(ethylene-glycol) (PEG)-PLA nanoparticles also use the clathrin-mediated pathway in HeLa cells, whereas anionic PEG-PLA nanoparticles do not.<sup>53</sup> Polystyrene nanoparticles appear to translocate across rat alveolar epithelial cell monolayers by an endocytosis-independent, transcellular pathway.<sup>54</sup> Other factors that may influence endocytosis of nanoparticles are their formulation and surface group modifications. It is generally assumed that the addition of one or more targeting moieties may facilitate retargeting of the core nanoparticle away from the default pathway and to a new one, depending on the efficiency of coating of the targeting moiety, its accessibility to the targeted receptor, the strength of the interaction and the abundance of the targeted receptor.<sup>14, 46, 53, 55</sup> The findings on BNPs thus far suggest that BNPs comprised of the different MW polymers tested here may utilize similar trafficking pathways, suggesting that the features that dominate their behavior are associated with the surface characteristics of the particle rather than the small variations in size. Finally, nanoparticle internalization characteristics may vary depending upon whether the cells are transformed (like HeLa cells), or not, and may also vary with the cell cycle. Our work has focused on assessment of internalization in non-dividing, subconfluent but unsynchronized cells, but future analyses which compare the pathways in different states of the cell cycle may be of great interest.

### Cytotoxicity Assessment

Among the potential applications for use of biodegradable nanoparticles are biological imaging and sensing. For this reason, it was important that the cytotoxicity be evaluated. HeLa cells were exposed to various doses of BNP3 or BNP12 for various time periods and their viability was assayed using a viability/cytotoxicity kit. Approximately 60 percent of the cells incubated with BNPs were viable after 24 hrs of exposure, comparable to control cells not exposed to BNPs (Figure 11). Viability was reduced to ~60% in control cells due to the absence of serum, which we omitted in these studies so as to make the cytotoxicity assays comparable to those used for analysis of BNP uptake. This data suggests that the BNPs are not acutely cytotoxic.

### Conclusion

The first steps in demonstrating biological utility for a new nanoparticle formulation are the characterization of its properties when in biological environment(s) of interest, as well as the characterization of its interactions with this environment. The unique optical properties of nanoparticles must be sustainable within a biological milieu to be useful for biomedical diagnostic applications. Here we have demonstrated that the unique and photostable emission properties of BF<sub>2</sub>dbmPLA nanoparticles are discernable both in aqueous solution and *in situ* in live cells using multiphoton excitation. We have also shown the selective



endocytosis of BNPs, through a specific mechanism, and the ability of the cells to tolerate high doses of BNPs for up to 24 hrs in culture. These studies, collectively, suggest that BNPs are useful, non-toxic agents for further development in the investigation of intracellular environments and trafficking pathways.

The next step in characterization of the endogenous internalization mechanism in these fibroblastic cells will logically involve utilization of molecular constructs allowing manipulation of different effector pathways, and assessment of co-localization of BNPs *in situ* with additional live cell membrane compartment markers. Likewise, investigation of the dynamics of BNP trafficking within cells expressing fluorescent tubulin and actin will enable visualization of intracellular movement in real time with respect to other membrane and structural markers. An equally important question that remains to be addressed is whether BNPs can be successfully redirected from their default pathway, characterized here in HeLa cells, to other endocytic pathways so as to expand their potential utility as probes. Utilization of the unique optical properties of BNP would ideally involve the attachment of targeting ligands, which may direct these moieties to diverse intracellular environments, as probes to explore microenvironments and their dynamic properties, including local oxygen concentrations and ways that they change over time. Another attractive application of the bright, color-tunable BNPs is that conjugating the BNPs of different molecular weights to different ligands of interest would enable the performance of multiplex studies.

Since no toxicity has been reported at high doses of BNPs in cultured cells, these particles exhibit characteristics *in vitro* that may be preferable relative to alternative nanoparticles such as quantum dots, whose core structure is relatively more toxic and toxicity is generally poorly studied.<sup>56-57</sup> For example, BNPs are two-photon excitable, bright, and also degradable. These properties are particularly useful for *in vivo* applications. The relative ease of preparation and cost effectiveness suggest great value in the further investigation and application of BNPs in diverse *in vitro* and *in vivo* situations which require photostable, inexpensive and modifiable nanoparticles to probe diverse environments. The demonstration that they are excitable using multiphoton excitation, also in this study, extends their applicability into animal models and even into the clinical setting.

## Methods

### Reagents

3,6-Dimethyl-1,4-dioxane-2,5-dione (D,L-lactide, Aldrich) was recrystallized twice from ethyl acetate and stored under nitrogen. Solvents, CH<sub>2</sub>Cl<sub>2</sub> and THF, were dried and purified by passing through alumina columns. Tin(II) 2-ethylhexanoate (Sn(oct)<sub>2</sub>, Spectrum), boron trifluoride diethyl etherate (Aldrich, purified, redistilled), and all other reagents and solvents were used as received without further purification. DbmOH,<sup>58</sup> BF<sub>2</sub>dbmOH,<sup>6</sup> and BF<sub>2</sub>dbmPLA<sup>6</sup> samples of different molecular weights<sup>11</sup> were prepared as previously reported. Dialysis tubing (Spectrum, volume/length: 6.4 ml/cm, MWCO: 12 – 14000) was washed and soaked in distilled H<sub>2</sub>O overnight before use. Nanoparticles were fabricated as previously described<sup>12</sup>. Methyl- $\beta$ -cyclodextrin (MBCD) was purchased from Sigma-Aldrich. Texas Red-EGF (TR-EGF), LysoTracker™ Red DND-99, LysoTracker™ Blue DND-22, AF594-Cholera toxin B, nocodazole, and the LIVE/DEAD viability/cytotoxicity kit for mammalian cells were all purchased from Invitrogen. Latrunculin B (Lat B) was purchased from Calbiochem.

### Characterization of Nanoparticles

UV/vis spectra were recorded on a Hewlett-Packard 8452A diode-array spectrophotometer. Molecular weights were determined by GPC (THF, 20°C, 1.0 mL/min) vs polystyrene

standards with RI and UV/vis detection ( $\lambda = 396$  nm for BF<sub>2</sub>dbmPLA), and a correction factor of 0.58 was applied to all data, as previously described.<sup>4</sup> Polymer Labs 5 $\mu$ m mixed-C columns along with Hewlett-Packard instrumentation (Series 1100 HPLC) and Viscotek software (TriSEC GPC Version 3.0, Viscotek Corp) were used in the GPC/RI or GPC/UV analysis. Nanoparticle sizes were determined by dynamic light scattering (DLS) (90° angle) on the Photocor Complex (Photocor Instruments Inc., USA) equipped with a He-Ne laser (Coherent, USA, Model 31-2082, 632.8 nm, 10 mW). Size and polydispersity analysis were performed using DynaLS software (Alango, Israel). The suspension was analyzed as such or diluted (0.5 mL) in H<sub>2</sub>O (9.5 mL). Photographs of nanoparticles were taken in the dark using a Casio Exilim Zoom EX-Z850 camera with the automatic setting (no flash).

### Acquisition of Luminescence Spectra

Emission spectra for the BNP suspensions were recorded with an Ocean Optics USB2000 Fiber Optic Spectrometer after excitation with a handheld UV lamp ( $\lambda_{\text{ex}} = 365$  nm; long wavelength setting). A ~500 ms delay was employed in collecting delayed emission spectra (i.e. delayed fluorescence and phosphorescence).

### Cell Culture

HeLa cells were obtained from the American Type Culture Collection (ATCC) and were cultured in a humidified incubator at 37°C in 95% air/5% CO<sub>2</sub> in phenol red-free Dulbecco's modified essential medium (DMEM)(4.5 g/L glucose with 10% FBS, 1% glutamine, and 1% non-essential amino acids) and split with trypsin/EDTA as recommended by the manufacturer. Cells were routinely analyzed at low passage in the subconfluent state although they were not synchronized.

### Photostability Assays

For measurement of *in-vitro* photostability, different BNPs were assayed using a black flat-bottomed 96-well plate. BNPs were added dropwise (5  $\mu$ l of a 1 mg/ml stock) into 195  $\mu$ l room-temperature incubation buffer (phenol red-free, serum-free DMEM with 1% penicillin/streptomycin and 20 mM HEPES). Serum was omitted from the incubation buffer to prevent possible nanoparticle aggregation. LysoTracker™ Blue was used as a reference for a UV-excitable and photostable fluorophore (5  $\mu$ l of a 1 mM stock). Fluorescence intensity was measured at 0 hr using an Envision™ 2103 Multilabel Reader (Perkin Elmer, excitation filter: 340nm, emission filter: 460nm). The plate was exposed to direct UV light for 17 or 24 hrs and the fluorescence intensity measured again as before. For *in-vivo* photostability studies, HeLa cells were seeded on 35mm glass-bottomed culture dishes at a density of  $8.5 \times 10^4$  cells/dish. On day 2 of culture, the cells were rinsed once with PBS and the medium replaced with cold incubation buffer of the composition described above (800 $\mu$ l). BNPs were added drop-wise (200 $\mu$ l) and incubated at 4°C for 1 hr. Unbound BNPs were rinsed off gently using PBS, the incubation buffer replaced (1 ml) and the cells incubated at 37°C for 1 hr. For reference, LysoTracker™ Blue (2.5  $\mu$ M final concentration) was added to cells after initial rinse and the cells incubated at 37°C for 1 hr. Following the 37°C incubation, the cells were rinsed four times with PBS and imaged. The BNPs or LysoTracker™ Blue were imaged using time series sequential bleach settings. For each cycle, the image was acquired using a line 4 average, which was followed by 10 iterations of bleaching using the 790 nm line at 4% power (74mW). Bleaching was started after one scan and repeated after one scan. Time-lapse imaging was performed using a Zeiss LSM 510 Meta NLO imaging system equipped with a Chameleon multiphoton laser mounted on a vibration-free table.

## Uptake Assays

HeLa cells were seeded on 6-well plates at a density of  $1.5 \times 10^5$  cells/well. On day 2 of culture, cells were rinsed briefly with phosphate-buffered saline (PBS) containing 1 mM  $\text{CaCl}_2$  and 0.5 mM  $\text{MgCl}_2$  and the media replaced with incubation buffer (900  $\mu\text{l}$ ) with or without MBCD (5 mM) or Lat B (2  $\mu\text{M}$ ) and incubated at  $37^\circ\text{C}$  for 30 min. After cooling on ice for 10 min, BNPs (100  $\mu\text{l}$ ) were added drop-wise and incubated at  $4^\circ\text{C}$  for 1 hr. For nocodazole pre-treatment, 33  $\mu\text{M}$  nocodazole was added prior to incubation at  $4^\circ\text{C}$ . Unbound BNPs were rinsed off with a gentle PBS ( $+\text{Ca}^{2+}$ ,  $+\text{Mg}^{2+}$ ) wash, the incubation buffer was replaced, and the cells were warmed to  $37^\circ\text{C}$  for various times up to 1 hr. After incubation, the cells were incubated with an ice-cold mild acidic wash buffer (0.1 M Sodium acetate, 0.05 M NaCl, pH 5.5) for 10 min at  $4^\circ\text{C}$ . Following the acid wash, the cells were washed three times with ice-cold PBS ( $+\text{Ca}^{2+}$ ,  $+\text{Mg}^{2+}$ ). To collect the cells, 700  $\mu\text{l}$  trypsin ( $37^\circ\text{C}$ ) were added to each well and incubated at  $37^\circ\text{C}$  for 3 min. The cells were then transferred to 1.5 ml eppendorf tubes and centrifuged for 5 min at 800 rpm at  $4^\circ\text{C}$ . The cell pellet was resuspended in 0.5 ml ice-cold PBS (without  $\text{Ca}^{2+}$  or  $\text{Mg}^{2+}$ ), filtered through a 70  $\mu\text{m}$  nylon filter and the fluorescence intensity measured by flow cytometry.

## Confocal and Multiphoton Fluorescence Microscopy

For BNP uptake studies, HeLa cells were seeded on 35 mm glass-bottom culture dishes at a density of  $8.5 \times 10^4$  cells/dish. On day 2 of culture, the cells were rinsed with PBS prior to addition of BNPs dropwise (200  $\mu\text{l}$ ) with incubation at  $4^\circ\text{C}$  for 1 hr. Unbound BNPs were rinsed off with a gentle PBS wash, the incubation buffer replaced, and the cells warmed to  $37^\circ\text{C}$  for various times up to 4 hr in the absence or presence of treatments. After incubation, the cells were rinsed four times with PBS and imaged with a Zeiss LSM 510 Meta NLO imaging system equipped with a Coherent Chameleon multiphoton laser mounted on a vibration-free table. For most studies, BNPs were excited in intact cells using the 790 nm line of the multiphoton laser. For assessment of co-localization of BNP and LysoTracker<sup>TM</sup> Red or AF594-Cholera toxin B in live cells, we utilized a Zeiss LSM 510 confocal microscope equipped with UV, Argon and green HeNe lasers for confocal fluorescence microscopy. For MBCD or Lat B pre-treatment, 5 mM MBCD or 2  $\mu\text{M}$  Lat B was added for 30 min at  $37^\circ\text{C}$  prior to addition of BNPs. For nocodazole treatment, 33  $\mu\text{M}$  nocodazole was added with the BNPs prior to incubation at  $4^\circ\text{C}$ . For colocalization studies, LysoTracker<sup>TM</sup> Red (50 nM), AF594-Cholera toxin B (10  $\mu\text{g}/\text{ml}$ ), or TR-EGF (200 ng/ml) was added to cells prior to incubation at  $37^\circ\text{C}$ . For immunostaining, following treatment with either 33  $\mu\text{M}$  nocodazole or 2  $\mu\text{M}$  Lat B, the cells were fixed in 4% paraformaldehyde prior to the addition of mouse monoclonal antibody to  $\alpha$ -tubulin and appropriate secondary fluorophore-conjugated antibody.

## Cytotoxicity Assays

HeLa cells were seeded on 96-well plates at a density of  $8 \times 10^3$  cells/well. On day 1 of culture, the cells were rinsed briefly in 200  $\mu\text{l}$  ice-cold PBS ( $+\text{Ca}^{2+}$ ,  $+\text{Mg}^{2+}$ ). Varying concentrations of BNPs (20  $\mu\text{g}/\text{ml}$ -200  $\mu\text{g}/\text{ml}$ ) in incubation buffer (phenol red-free, serum-free DMEM with 1% P/S and 20 mM HEPES) were added drop-wise (200  $\mu\text{l}$  total volume) and incubated on ice for 1 hr. Following the incubation, the cells were washed once in 200  $\mu\text{l}$  ice-cold PBS ( $+\text{Ca}^{2+}$ ,  $+\text{Mg}^{2+}$ ), the media replaced with 200  $\mu\text{l}$   $37^\circ\text{C}$  incubation buffer, and the plate incubated at  $37^\circ\text{C}$  for various time points (1-24 hrs). Calcein (494/517 nm) and Ethidium homodimer-1 (528/617 nm) provided in the LIVE/DEAD cell assay kit (Invitrogen) were used to detect live/dead cells and were added to cells after the incubation (50  $\mu\text{l}$  of 0.5  $\mu\text{M}$  calcein AM and 1.5  $\mu\text{M}$  EthD-1). Fluorescence intensity was measured using an Envision<sup>TM</sup> 2103 Multilabel Reader (Perkin Elmer).

## Statistics

Cells from each experiment were analyzed individually and the results from different experiments were compared using the Student's t-test with  $p \leq 0.05$  to evaluate the statistical significance of any observed changes.

## Supplementary Material

Refer to Web version on PubMed Central for supplementary material.

## Acknowledgments

We thank the National Science Foundation (CLF: BES 0402212, CHE-0718879), the UVA nanoSTAR Institute (CLF: seed grant) and the National Institutes of Health (SHA: RO1 EY017293) for support for this work. We also thank the USC Center for Liver Diseases (P30 DK048522) for access to the Cell Biology Core Facility. We gratefully acknowledge the Harrison Undergraduate Research Program at UVA for a research award to YJC and the National Institutes of Health for a Ruth Kirchstein Predoctoral Fellowship for JC (F31EY018807).

## References

1. Torchilin VP. Fluorescence Microscopy to Follow the Targeting of Liposomes and Micelles to Cells and Their Intracellular Fate. *Adv Drug Deliv Rev.* 2005; 57:95–109. [PubMed: 15518923]
2. Cochran DM, Fukumura D, Ancukiewicz M, Carmeliet P, Jain RK. Evolution of Oxygen and Glucose Concentration Profiles in a Tissue-Mimetic Culture System of Embryonic Stem Cells. *Ann Biomed Eng.* 2006; 34:1247–58. [PubMed: 16832606]
3. Sanchez JM, Sacks RD. Development of a Multibed Sorption Trap, Comprehensive Two-Dimensional Gas Chromatography, and Time-of-Flight Mass Spectrometry System for the Analysis of Volatile Organic Compounds in Human Breath. *Anal Chem.* 2006; 78:3046–54. [PubMed: 16642992]
4. Vanderkooi JM, Maniara G, Green TJ, Wilson DF. An Optical Method for Measurement of Dioxygen Concentration Based Upon Quenching of Phosphorescence. *J Biol Chem.* 1987; 262:5476–82. [PubMed: 3571219]
5. Zhang G, Palmer GM, Dewhirst MW, Fraser CL. A Dual-Emissive-Materials Design Concept Enables Tumour Hypoxia Imaging. *Nat Mater.* 2009; 8:747–51. [PubMed: 19668206]
6. Zhang G, Chen J, Payne SJ, Kooi SE, Demas JN, Fraser CL. Multi-Emissive Difluoroboron Dibenzoylmethane Polylactide Exhibiting Intense Fluorescence and Oxygen-Sensitive Room-Temperature Phosphorescence. *J Am Chem Soc.* 2007; 129:8942–3. [PubMed: 17608480]
7. Griffith LG, Naughton G. Tissue Engineering--Current Challenges and Expanding Opportunities. *Science.* 2002; 295:1009–14. [PubMed: 11834815]
8. Chow YL, Johansson CI, Zhang YH, Gautron R, Yang L, Rassat A, Yang SZ. Spectroscopic and Electrochemical Properties of 1,3-Diketoneboron Derivatives. *J Phys Org Chem.* 1996; 9:7–16.
9. Cogne-Laage E, Allemand JF, Ruel O, Baudin JB, Croquette V, Blanchard-Desce M, Jullien L. Diaryloxy(Methanato)Boron Difluoride Compounds as Medium-Sensitive Two-Photon Fluorescent Probes. *Chemistry.* 2004; 10:1445–55. [PubMed: 15034888]
10. Loudet A, Burgess K. BODIPY Dyes and Their Derivatives: Syntheses and Spectroscopic Properties. *Chem Rev.* 2007; 107:4891–932. [PubMed: 17924696]
11. Zhang G, Kooi SE, Demas JN, Fraser CL. Emission Color Tuning with Polymer Molecular Weight for Difluoroboron Dibenzoylmethane-Polylactide. *Adv Mater.* 2008; 20:2099–104.
12. Pfister A, Zhang G, Zareno J, Horwitz AF, Fraser CL. Boron Polylactide Nanoparticles Exhibiting Fluorescence and Phosphorescence in Aqueous Medium. *ACS Nano.* 2008; 2:1252–8. [PubMed: 19081748]
13. Farokhzad OC, Langer R. Nanomedicine: Developing Smarter Therapeutic and Diagnostic Modalities. *Adv Drug Deliv Rev.* 2006; 58:1456–9. [PubMed: 17070960]
14. Whitesides GM. Nanoscience, Nanotechnology, and Chemistry. *Small.* 2005; 1:172–9. [PubMed: 17193427]

15. Buono C, Anzinger JJ, Amar M, Kruth HS. Fluorescent Pegylated Nanoparticles Demonstrate Fluid-Phase Pinocytosis by Macrophages in Mouse Atherosclerotic Lesions. *J Clin Invest.* 2009; 119:1373–81. [PubMed: 19363293]
16. Williams Y, Byrne S, Bashir M, Davies A, Whelan A, Gun'ko Y, Kelleher D, Volkov Y. Comparison of Three Cell Fixation Methods for High Content Analysis Assays Utilizing Quantum Dots. *J Microsc.* 2008; 232:91–8. [PubMed: 19017205]
17. Conner SD, Schmid SL. Regulated Portals of Entry Into the Cell. *Nature.* 2003; 422:37–44. [PubMed: 12621426]
18. Doherty GJ, McMahon HT. Mechanisms of Endocytosis. *Annu Rev Biochem.* 2009; 78:857–902. [PubMed: 19317650]
19. Kirchhausen T, Macia E, Pelish HE. Use of Dynasore, the Small Molecule Inhibitor of Dynamin, in the Regulation of Endocytosis. *Methods Enzymol.* 2008; 438:77–93. [PubMed: 18413242]
20. Macia E, Ehrlich M, Massol R, Boucrot E, Brunner C, Kirchhausen T. Dynasore, a Cell-Permeable Inhibitor of Dynamin. *Dev Cell.* 2006; 10:839–50. [PubMed: 16740485]
21. Thompson HM, McNiven MA. Discovery of a New 'Dynasore'. *Nat Chem Biol.* 2006; 2:355–6. [PubMed: 16783339]
22. Kirkham M, Parton RG. Clathrin-Independent Endocytosis: New Insights Into Caveolae and Non-Caveolar Lipid Raft Carriers. *Biochimica et biophysica acta.* 2005; 1745:273–86. [PubMed: 16046009]
23. Kiss AL, Botos E. Endocytosis Via Caveolae: Alternative Pathway with Distinct Cellular Compartments to Avoid Lysosomal Degradation? *J Cell Mol Med.* 2009; 13:1228–37. [PubMed: 19382909]
24. Le PU, Nabi IR. Distinct Caveolae-Mediated Endocytic Pathways Target the Golgi Apparatus and the Endoplasmic Reticulum. *J Cell Sci.* 2003; 116:1059–71. [PubMed: 12584249]
25. Parton RG, Simons K. The Multiple Faces of Caveolae. *Nat Rev Mol Cell Biol.* 2007; 8:185–94. [PubMed: 17318224]
26. Rodal SK, Skretting G, Garred O, Vilhardt F, van Deurs B, Sandvig K. Extraction of Cholesterol with Methyl-Beta-Cyclodextrin Perturbs Formation of Clathrin-Coated Endocytic Vesicles. *Molecular biology of the cell.* 1999; 10:961–74. [PubMed: 10198050]
27. Abban CY, Bradbury NA, Meneses PI. HPV16 and BPV1 Infection can be Blocked by the Dynamin Inhibitor Dynasore. *Am J Ther.* 2008; 15:304–11. [PubMed: 18645330]
28. Dausend J, Musyanovych A, Dass M, Walther P, Schrezenmeier H, Landfester K, Mailander V. Uptake Mechanism of Oppositely Charged Fluorescent Nanoparticles in HeLa Cells. *Macromol Biosci.* 2008; 8:1135–43. [PubMed: 18698581]
29. Huang F, Khvorova A, Marshall W, Sorkin A. Analysis of Clathrin-Mediated Endocytosis of Epidermal Growth Factor Receptor by RNA Interference. *J Biol Chem.* 2004; 279:16657–61. [PubMed: 14985334]
30. Young A, Gentzsch M, Abban CY, Jia Y, Meneses PI, Bridges RJ, Bradbury NA. Dynasore Inhibits Removal of Wild-Type and DeltaF508 Cystic Fibrosis Transmembrane Conductance Regulator (CFTR) From the Plasma Membrane. *Biochem J.* 2009; 421:377–85. [PubMed: 19442237]
31. Sorkin A, Goh LK. Endocytosis and Intracellular Trafficking of ErbBs. *Exp Cell Res.* 2009; 315:683–96. [PubMed: 19278030]
32. Kumari S, Mayor S. ARF1 is Directly Involved in Dynamin-Independent Endocytosis. *Nat Cell Biol.* 2008; 10:30–41. [PubMed: 18084285]
33. Da Costa SR, Yarber FA, Zhang L, Sonoe M, Hamm-Alvarez SF. Microtubules Facilitate the Stimulated Secretion of Beta-Hexosaminidase in Lacrimal Acinar Cells. *Journal of cell science.* 1998; 111:1267–76. [PubMed: 9547304]
34. Mush A. Microtubule Organization and Function in Epithelial Cells. *Traffic.* 2004; 5:1–9. [PubMed: 14675420]
35. Jerdeva GV, Wu K, Yarber FA, Rhodes CJ, Kalman D, Schechter JE, Hamm-Alvarez SF. Actin and Non-Muscle Myosin II Facilitate Apical Exocytosis of Tear Proteins in Rabbit Lacrimal Acinar Epithelial Cells. *Journal of cell science.* 2005b; 118:4797–812. [PubMed: 16219687]



36. Bayer N, Schober D, Prchla E, Murphy RF, Blaas D, Fuchs R. Effect of Bafilomycin A1 and Nocodazole on Endocytic Transport in HeLa Cells: Implications for Viral Uncoating and Infection. *J Virol*. 1998; 72:9645–55. [PubMed: 9811698]
37. Ferreira D, Cortez M, Atayde VD, Yoshida N. Actin Cytoskeleton-Dependent and -Independent Host Cell Invasion by *Trypanosoma cruzi* is Mediated by Distinct Parasite Surface Molecules. *Infect Immun*. 2006; 74:5522–8. [PubMed: 16988227]
38. Zieve GW. Nocodazole and Cytochalasin D Induce Tetraploidy in Mammalian Cells. *Am J Physiol*. 1984; 246:C154–6. [PubMed: 6696055]
39. Apodaca G. Endocytic Traffic in Polarized Epithelial Cells: Role of the Actin and Microtubule Cytoskeleton. *Traffic*. 2001; 2:149–59. [PubMed: 11260520]
40. Wood SA, Brown WJ. The Morphology But Not the Function of Endosomes and Lysosomes is Altered by Brefeldin A. *J Cell Biol*. 1992; 119:273–85. [PubMed: 1400573]
41. Nel AE, Madler L, Velegol D, Xia T, Hoek EM, Somasundaran P, Klaessig F, Castranova V, Thompson M. Understanding Biophysicochemical Interactions at the Nano-Bio Interface. *Nat Mater*. 2009; 8:543–57. [PubMed: 19525947]
42. Chithrani BD, Chan WC. Elucidating the Mechanism of Cellular Uptake and Removal of Protein-Coated Gold Nanoparticles of Different Sizes and Shapes. *Nano Lett*. 2007; 7:1542–50. [PubMed: 17465586]
43. Harush O, Altschuler Y, Benita S. The Impact of Surface Charge on Nanoparticle Performance. 2007:85–102.
44. Harush-Frenkel O, Altschuler Y, Benita S. Nanoparticle-Cell Interactions: Drug Delivery Implications. *Crit Rev Ther Drug Carrier Syst*. 2008; 25:485–544. [PubMed: 19166392]
45. Harush-Frenkel O, Rozentur E, Benita S, Altschuler Y. Surface Charge of Nanoparticles Determines their Endocytic and Transcytotic Pathway in Polarized MDCK Cells. *Biomacromolecules*. 2008; 9:435–43. [PubMed: 18189360]
46. Hillaireau H, Couvreur P. Nanocarriers' Entry Into the Cell: Relevance to Drug Delivery. *Cell Mol Life Sci*. 2009; 66:2873–96. [PubMed: 19499185]
47. Lee KD, Hong K, Papahadjopoulos D. Recognition of Liposomes by Cells: In Vitro Binding and Endocytosis Mediated by Specific Lipid Headgroups and Surface Charge Density. *Biochim Biophys Acta*. 1992; 1103:185–97. [PubMed: 1543703]
48. Liu D, Song YK. Cationic Liposome-Mediated Transfection *In Vivo* (Review). *Gene Ther Mol Biol*. 1998; 2:59–68.
49. Kovacs T, Karasz A, Szollosi J, Nagy P. The Density of GM1-Enriched Lipid Rafts Correlates Inversely with the Efficiency of Transfection Mediated by Cationic Liposomes. *Cytometry A*. 2009; 75:650–7. [PubMed: 19526485]
50. Lai SK, Hida K, Man ST, Chen C, Machamer C, Schroer TA, Hanes J. Privileged Delivery of Polymer Nanoparticles to the Perinuclear Region of Live Cells Via a Non-Clathrin, Non-Degradative Pathway. *Biomaterials*. 2007; 28:2876–84. [PubMed: 17363053]
51. Panyam J, Labhasetwar V. Dynamics of Endocytosis and Exocytosis of Poly(D,L-lactide-co-glycolide) Nanoparticles in Vascular Smooth Muscle Cells. *Pharm Res*. 2003; 20:212–20. [PubMed: 12636159]
52. Panyam J, Zhou WZ, Prabha S, Sahoo SK, Labhasetwar V. Rapid Endo-Lysosomal Escape of poly(DL-lactide-co-glycolide) Nanoparticles: Implications for Drug and Gene Delivery. *Faseb J*. 2002; 16:1217–26. [PubMed: 12153989]
53. Harush-Frenkel O, Debotton N, Benita S, Altschuler Y. Targeting of Nanoparticles to the Clathrin-Mediated Endocytic Pathway. *Biochem Biophys Res Commun*. 2007; 353:26–32. [PubMed: 17184736]
54. Yacobi NR, M N, Fazlollahi F, DeMaio L, Marchelletta R, Hamm-Alvarez SF, Borok Z, Kim KJ, Crandall ED. Mechanisms of Alveolar Epithelial Translocation of a Defined Population of Nanoparticles. *Am J Respir Cell Mol Biol*. 2009
55. Bareford LM, Swaan PW. Endocytic Mechanisms for Targeted Drug Delivery. *Adv Drug Deliv Rev*. 2007; 59:748–58. [PubMed: 17659804]
56. Chang E, Thekkekk N, Yu WW, Colvin VL, Drezek R. Evaluation of Quantum Dot Cytotoxicity Based on Intracellular Uptake. *Small*. 2006; 2:1412–7. [PubMed: 17192996]



57. Jamieson T, Bakhshi R, Petrova D, Pocock R, Imani M, Seifalian AM. Biological Applications of Quantum Dots. *Biomaterials*. 2007; 28:4717–32. [PubMed: 17686516]
58. Bender JL, Corbin PS, Fraser CL, Metcalf DH, Richardson FS, Thomas EL, Urbas AM. Site-Isolated Luminescent Europium Complexes with Polyester Macroligands: Metal-Centered Heteroarm Stars and Nanoscale Assemblies with Labile Block Junctions. *J Am Chem Soc*. 2002; 124:8526–7. [PubMed: 12121083]

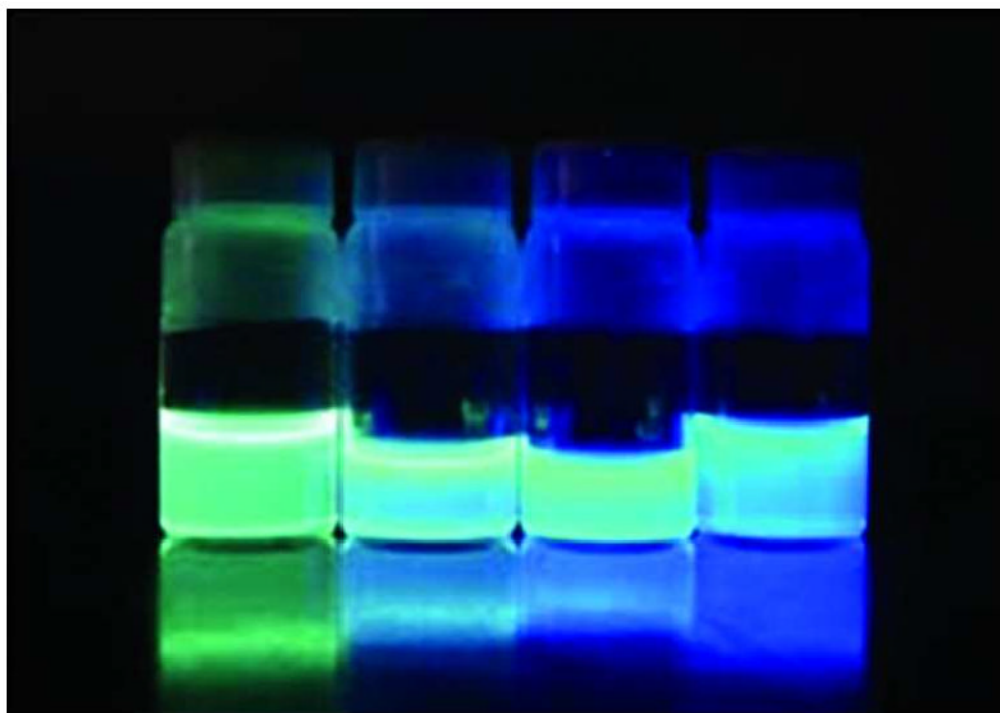


**Figure 1.** Image of BNP suspensions fabricated from polymers of different molecular weights (left to right, MW (kDa): 3, 6, 13, 20) showing green to blue emission color tuning ( $\lambda_{\text{ex}} = 365 \text{ nm}$ ).

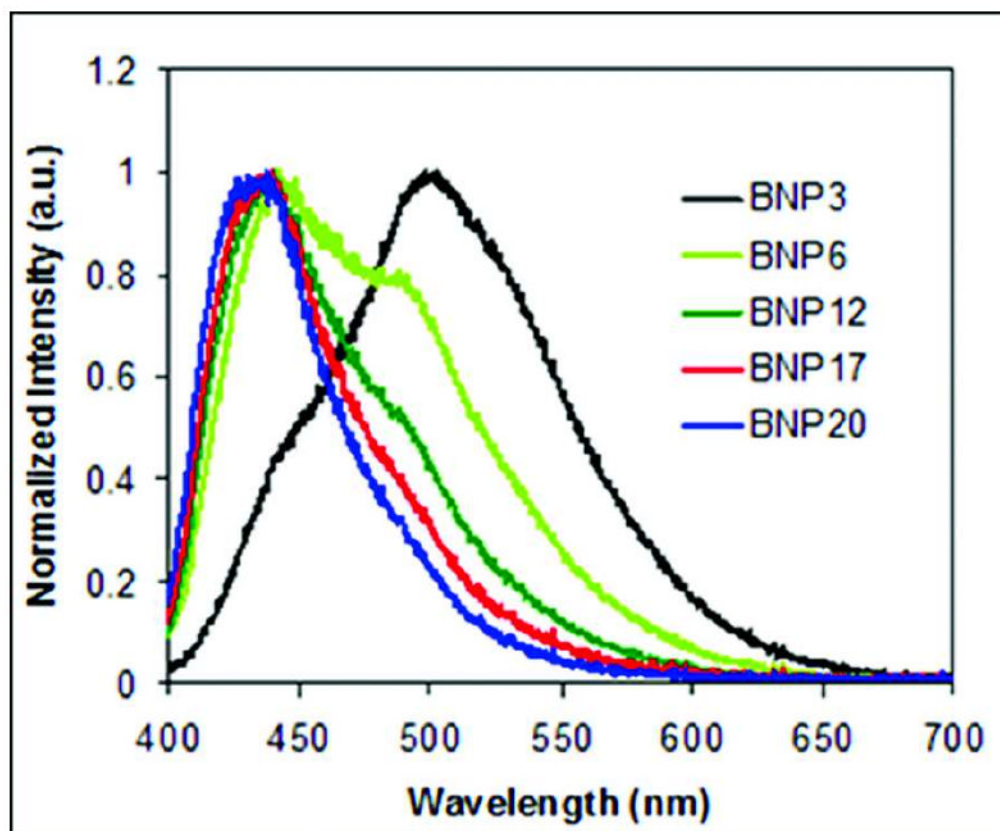


**Figure 2.**  
Fluorescence spectra of aqueous BNP suspensions ( $\lambda_{\text{ex}} = 365$  nm).

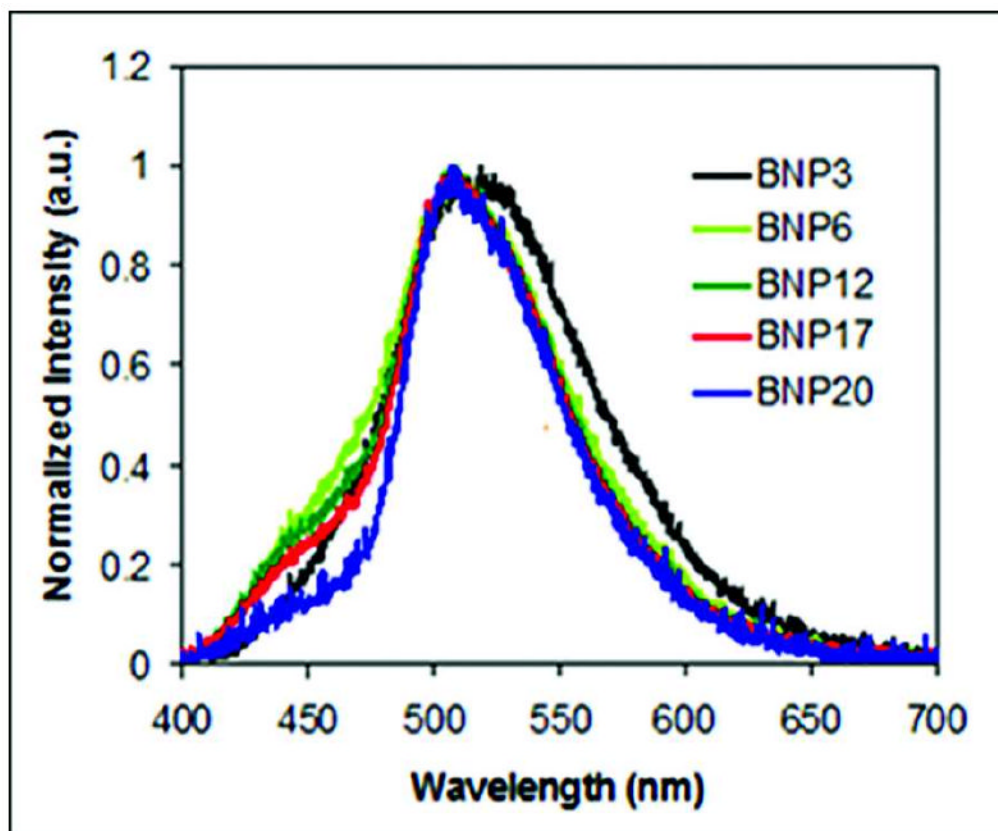


**Figure 3.** Delayed emission spectra for the BNP series. Delayed fluorescence (DF) (shoulder at  $\lambda \sim 440\text{-}465$  nm) and room temperature phosphorescence (RTP) ( $\lambda \sim 508\text{-}519$  nm) ( $\lambda_{\text{ex}} = 365$  nm;  $\sim 500$  ms delay).

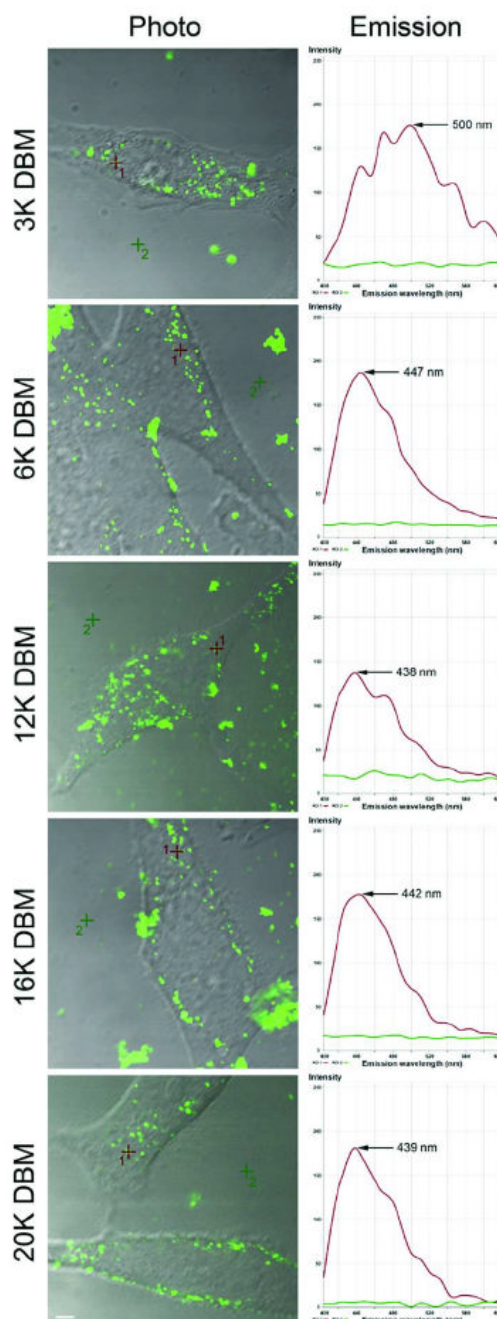
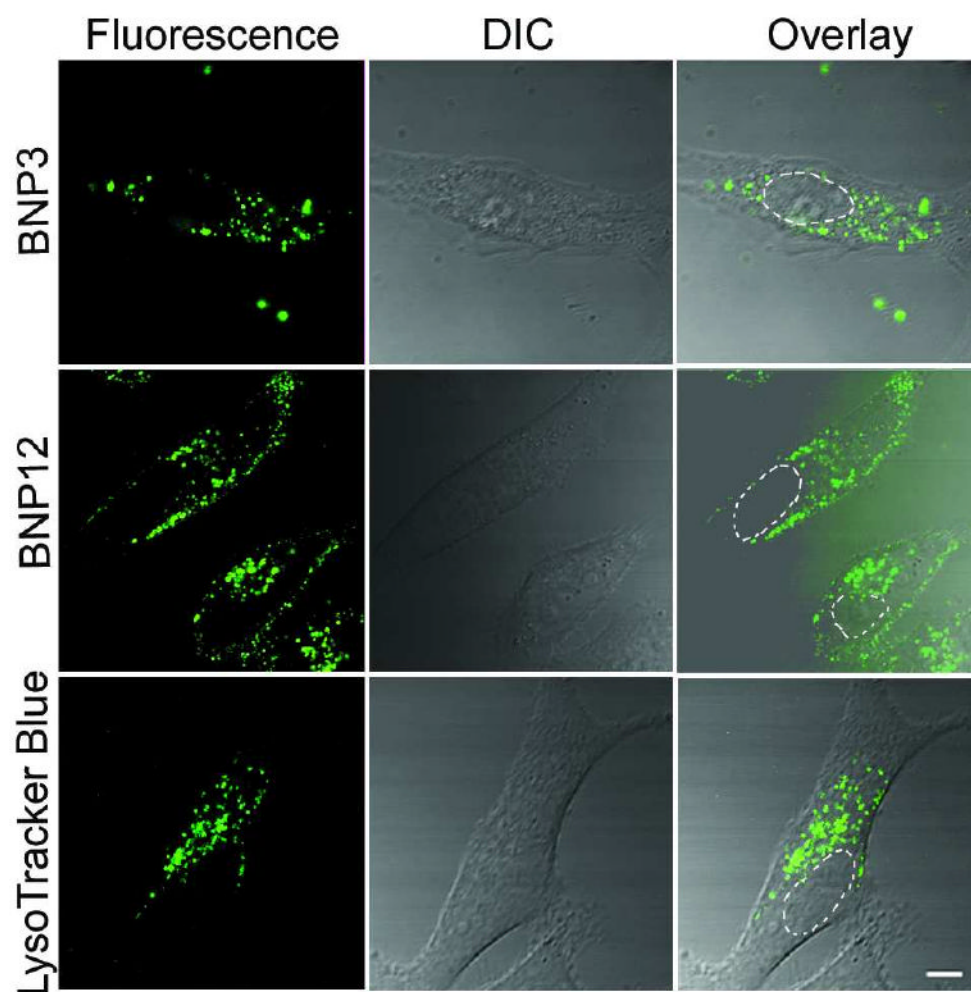


**Figure 4.**

BNP distribution and intracellular emission spectra in HeLa cells. *Left column:* BNPs of different molecular weights show comparable punctate intracellular distributions in HeLa cells. HeLa cells were incubated with 200  $\mu\text{g}/\text{ml}$  BNPs of different molecular weights for 1 hr at 37°C. After incubation, the BNPs were excited using the 790 nm line of a Chameleon multiphoton laser while emitted light was restricted in channel mode to a narrow range corresponding to the *in-vitro* fluorescence emission spectrum of these particles, from 460–550 nm for BNP3 and from 420–485 nm for BNP6, BNP12, BNP17 and BNP20. *Right column:* BNPs were excited using the 790 nm line of a Chameleon multiphoton laser and emission was calculated in lambda mode for acquisition of a spectral emission signal

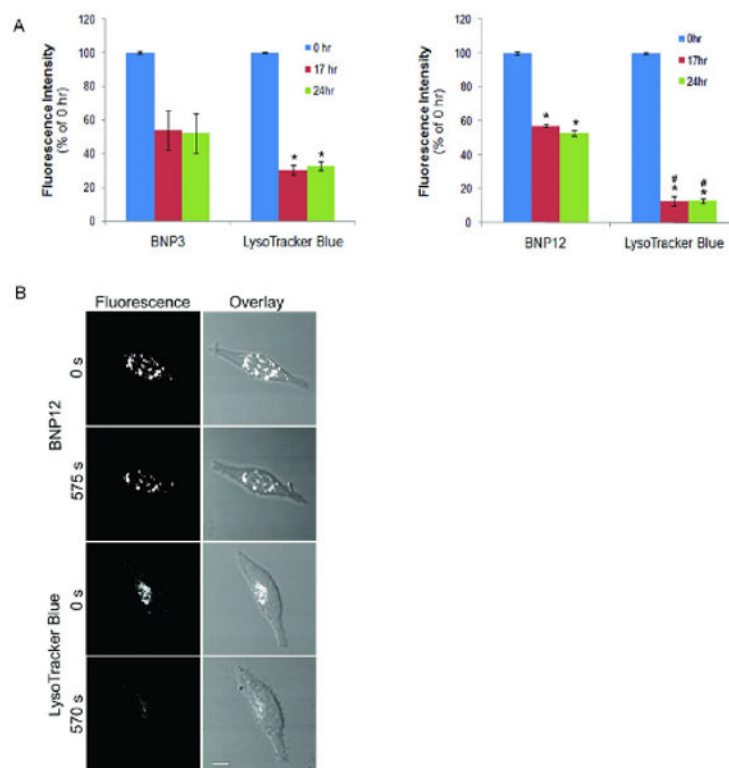
ranging from 400-600 nm. Spectra corresponding to the numbered points on the image to the left are shown on the right with “1” denoting a region filled with a nanoparticle and “2” denoting background. Bar, 5  $\mu\text{m}$ .





**Figure 5.**

HeLa cell uptake of BNP3 and BNP12. HeLa cells were incubated with 200  $\mu\text{g/ml}$  BNP3 or BNP12 or with 2.5  $\mu\text{M}$  LysoTracker<sup>TM</sup> Blue, for 1 hr at 37°C and then imaged using confocal fluorescence microscopy. Excitation was at 790 nm for all markers. Emission was restricted to 460-550 nm for BNP3, 420-485 nm for BNP12, and 390-465 nm for LysoTracker<sup>TM</sup> Blue. Bar, 5  $\mu\text{m}$ . Dotted lines represent the nuclear region identified from the DIC image.

**Figure 6.**

BNP photostability. **A. In-vitro photostability.** BNPs (5  $\mu$ l of a 1 mg/ml stock) were added to a black, flat-bottomed 96-well plate and the fluorescence intensity measured at 0 hr. Following exposure to direct UV light for 17 and 24 hrs, the fluorescence intensity was measured again as before. LysoTracker™ Blue was used as a reference UV-excitable fluorophore. (n= 3 for both BNP3 and BNP12, \*,  $p \leq 0.05$  relative to controls and #,  $p \leq 0.05$  relative to BNP12). **B. In-vivo photostability.** HeLa cells seeded on glass-bottom culture dishes were incubated with either LysoTracker™ Blue or BNP12 and imaged over time as described in Materials and Methods. Bar, 5  $\mu$ m.

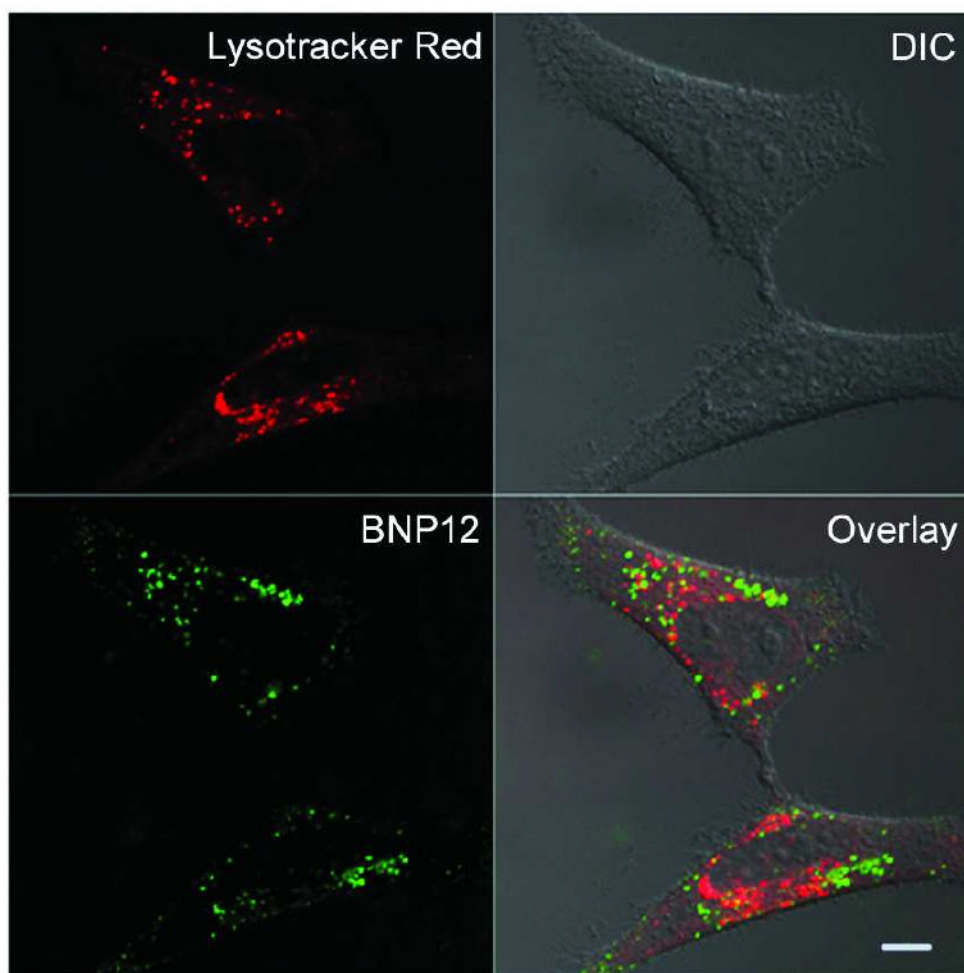


**Figure 7.**

BNPs are not markedly co-localized with lysosomal compartments. HeLa cells were incubated with BNP12 (200  $\mu\text{g/ml}$ ) and Lysotracker<sup>TM</sup> Red for 1 hr at 37°C as described in Materials and Methods and then imaged. A UV laser was used for excitation of nanoparticles (green) and a HeNe1 laser for excitation of LysoTracker<sup>TM</sup> Red (red). Bar, 5  $\mu\text{m}$ .

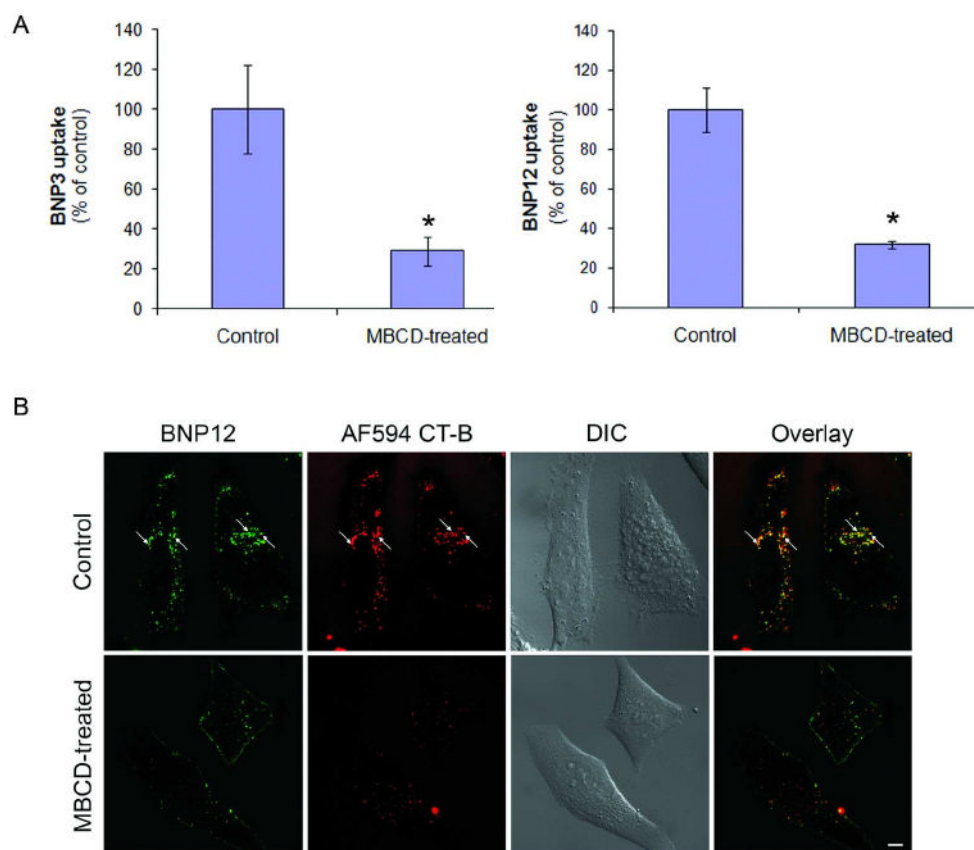


**Figure 8.**

Uptake of BNPs is inhibited by MBCD treatment. **A.** HeLa cells were untreated (control) or pre-treated with 5 mM MBCD for 30 min at 37°C prior to addition of BNP3 or BNP12 (200 µg/ml). Following uptake for 1 hr at 37°C, remaining surface-bound nanoparticles were removed by a mild acidic wash. The remaining cell-associated fluorescence signal was measured by flow cytometry using appropriate laser and filter settings. (n= 6 for BNP3 and n= 5 for BNP12, \*:  $p \leq 0.05$ ). **B.** HeLa cells were incubated with 200 µg/ml BNP12 and 10 µg/ml Alexa Fluor 594-conjugated cholera toxin subunit B (AF594 CT-B) for 1 hr at 37°C with or without 5 mM MBCD pre-treatment for 30 min at 37°C. A UV laser was used for excitation of BNP12 (green) and a HeNe1 laser for excitation of AF594 CT-B. Arrows: colocalization of boron nanoparticles (BNP12) and AF594 CT-B. Bar: 5 µm.

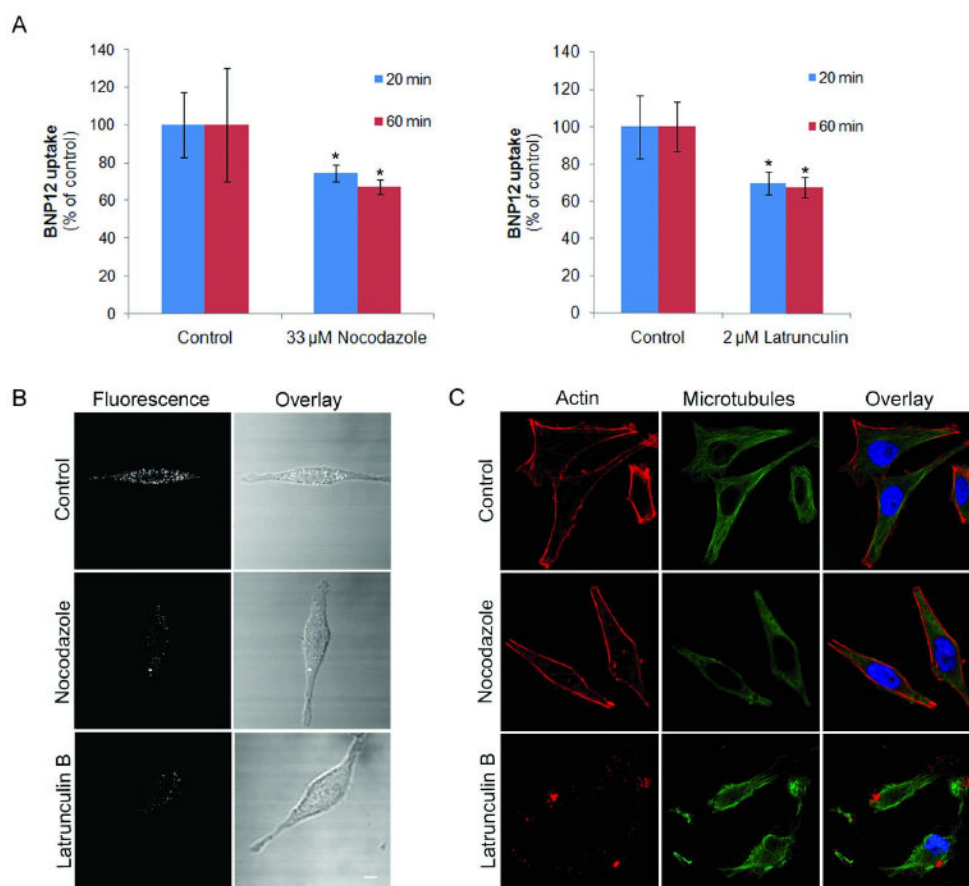


**Figure 9.**

Disruption of the cytoskeleton affects BNP uptake. **A.** HeLa cells were untreated (control) or pre-treated with either 33  $\mu$ M nocodazole or 2  $\mu$ M Lat B prior to addition of BNP12 (200  $\mu$ g/ml). Following uptake for 20 or 60 min at 37°C, remaining surface-bound BNPs were removed by mild acid wash. The signal was collected by flow cytometry using appropriate laser and filter settings. (n= 8 for 20 min and n= 6 for 60 min nocodazole; n= 12 for 20 min and n= 14 for 60 min Lat B. \*:  $p \leq 0.05$ ). **B.** HeLa cells were untreated (control) or pre-treated with either 33  $\mu$ M nocodazole or 2  $\mu$ M Lat B prior to addition of BNP12 (200  $\mu$ g/ml). Following uptake for 20 min at 37°C the cells were imaged using confocal laser microscopy. Excitation: 790 nm. Bar, 5  $\mu$ m. **C.** HeLa cells without any treatment (control) or treated with either 33  $\mu$ M nocodazole or 2  $\mu$ M Lat B for 60 min were fixed and labeled with a primary antibody to  $\alpha$ -tubulin (green) combined with an appropriate secondary antibody in parallel with rhodamine-phalloidin to label actin (red). Bar, 5  $\mu$ m.

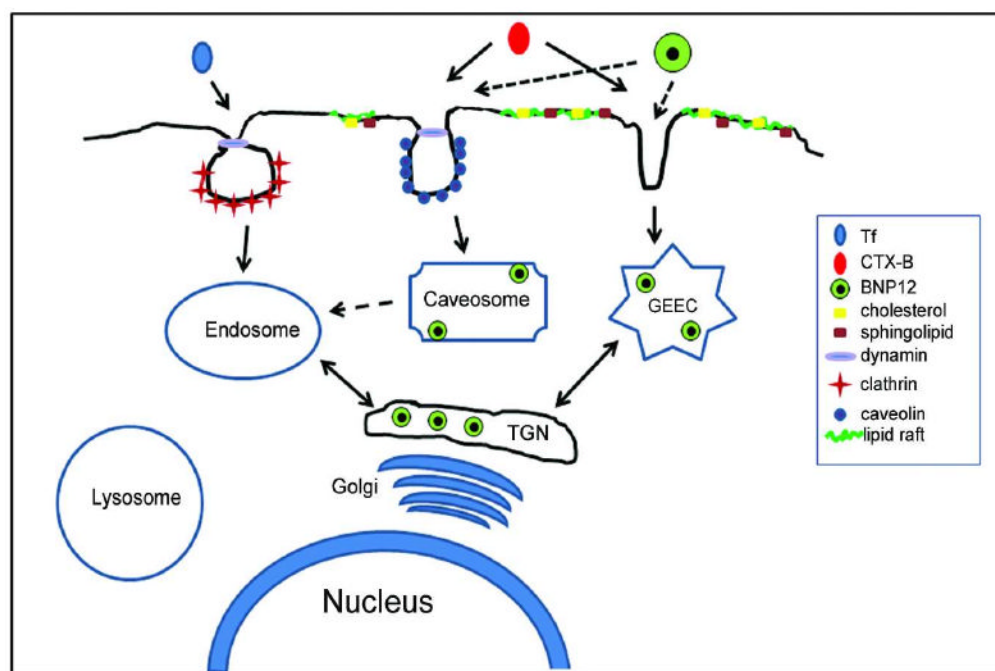


**Figure 10.**

Schematic diagram depicting BNP uptake through lipid raft-dependent internalization pathways that also serve as the routes of uptake for cholera toxin B (CT-B). The BNPs may ultimately reach the perinuclear trans-golgi network (TGN) by one of two pathways. The first is by direct communication between the GPI-AP-enriched early endosomal compartment (GEEC) and the TGN. The second is by communication between caveosomes and classical endosomes and subsequent communication between the latter and the TGN.



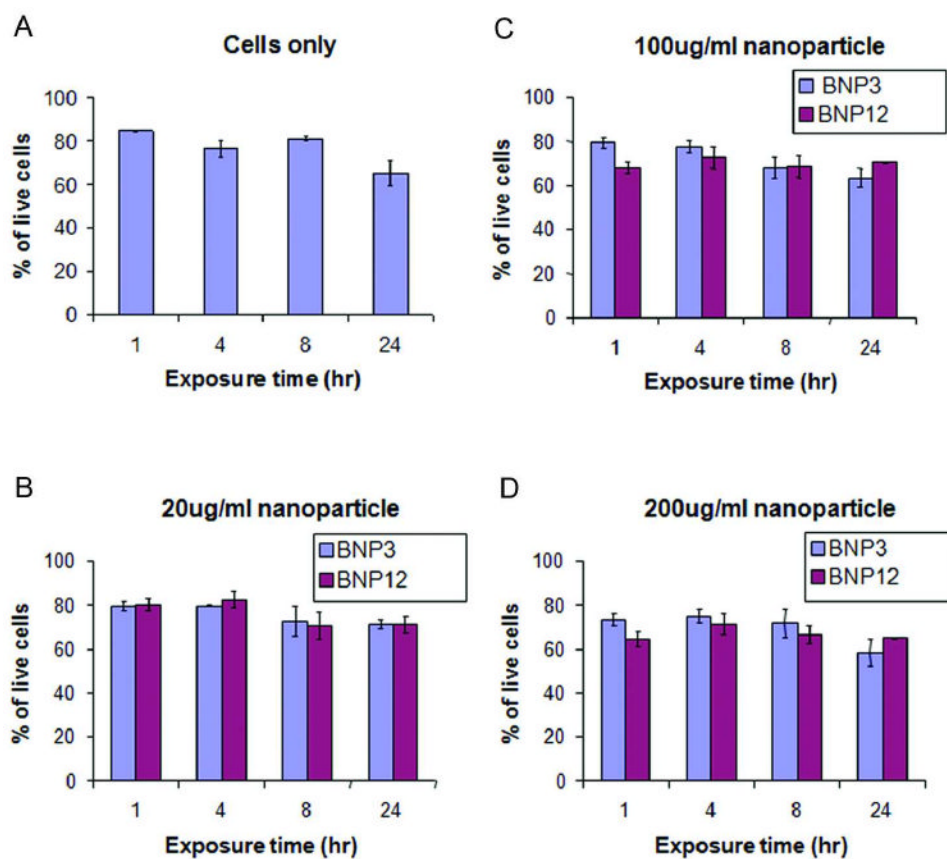


**Figure 11.**

BNP exposure does not affect cell viability. HeLa cells were exposed to culture medium (A), 20  $\mu\text{g/ml}$  (B), 100  $\mu\text{g/ml}$  (C), or 200  $\mu\text{g/ml}$  (D) of BNP3 or BNP12 for various time periods up to 24 hrs at 37°C. Cell viability was assayed using a LIVE/DEAD viability/cytotoxicity kit. (n=3).

Table 1

Boron Nanoparticle Characterization Data.

Sample	$M_n^a$ (kDa)	PDI <sup>b</sup>	$\epsilon$ before <sup>c</sup> ( $M^{-1}cm^{-1}$ )	$\epsilon$ after <sup>d</sup> ( $M^{-1}cm^{-1}$ )	Diameter <sup>e</sup> (nm)	PD <sup>e</sup>	$\lambda_{em} F/f$ (nm)	$\lambda_{em} P g$ (nm)
BNP3	3.0	1.11	44,900	42,800	96	0.22	498	519
BNP6	6.0	1.08	38,700	35,600	88	0.22	442	509
BNP12	12.3	1.11	38,300	36,500	85	0.06	440	509
BNP17	16.8	1.21	37,700	34,900	77	0.14	439	508
BNP20	20.2	1.63	27,700	25,100	95	0.21	437	508

<sup>a</sup>Determined by GPC in THF vs polystyrene standards.

<sup>b</sup>GPC PDI = polydispersity index

<sup>c</sup>BF<sub>2</sub>dbmPLA extinction coefficient at  $\lambda_{max}$  = 396 nm in CH<sub>2</sub>Cl<sub>2</sub>, before nanoparticle fabrication

<sup>d</sup>As in c for lyophilized samples after nanoparticle fabrication.

<sup>e</sup>Determined by dynamic light scattering. PD = polydispersity.

<sup>f</sup>Fluorescence emission maximum for aqueous nanoparticle suspension.

<sup>g</sup>Phosphorescence emission maximum for aqueous nanoparticle suspension.